

# Design of plasmonic toroidal metamaterials at optical frequencies

Yao-Wei Huang,<sup>1</sup> Wei Ting Chen,<sup>1</sup> Pin Chieh Wu,<sup>1,2</sup> Vassili Fedotov,<sup>3</sup> Vassili Savinov,<sup>3</sup>  
You Zhe Ho,<sup>2</sup> Yuan-Fong Chau,<sup>4</sup> Nikolay I. Zheludev,<sup>3</sup> and Din Ping Tsai<sup>1,2,5,6,\*</sup>

<sup>1</sup>Graduate Institute of Applied Physics, National Taiwan University, Taipei 10617, Taiwan

<sup>2</sup>Department of Physics, National Taiwan University, Taipei 10617, Taiwan

<sup>3</sup>Optoelectronics Research Centre and Centre for Photonic Metamaterials, University of Southampton, Southampton SO17 1BJ, UK

<sup>4</sup>Department of Electronic Engineering, Ching Yun University, Jung-Li 320, Taiwan

<sup>5</sup>Instrument Technology Research Center, National Applied Research Laboratories, Hsinchu 300, Taiwan

<sup>6</sup>Research Center for Applied Sciences, Academia Sinica, Taipei 115, Taiwan

\*[dptsai@phys.ntu.edu.tw](mailto:dptsai@phys.ntu.edu.tw)

**Abstract:** Toroidal multipoles are the subject of growing interest because of their unusual electromagnetic properties different from the electric and magnetic multipoles. In this paper, we present two new related classes of plasmonic metamaterial composed of purposely arranged of four U-shaped split ring resonators (SRRs) that show profound resonant toroidal responses at optical frequencies. The toroidal and magnetic responses were investigated by the finite-element simulations. A phenomenon of reversed toroidal responses at higher and lower resonant frequencies has also been reported between this two related metamaterials which results from the electric and magnetic dipoles interaction. Finally, we propose a physical model based on coupled LC circuits to quantitatively analyze the coupled system of the plasmonic toroidal metamaterials.

© 2012 Optical Society of America

**OCIS codes:** (160.3918) Metamaterials; (240.6680) Surface plasmons; (140.4780) Optical resonators; (250.5403) Plasmonics.

---

## References and links

1. I. A. Zel'dovich, "The relation between decay asymmetry and dipole moment of elementary particles," *Sov. Phys. JETP* **6**, 1184 (1958).
2. V. M. Dubovik and V. V. Tugushev, "Toroid moments in electrodynamics and solid-state physics," *Phys. Rep.* **187**(4), 145–202 (1990).
3. A. D. Boardman, K. Marinov, N. Zheludev, and V. A. Fedotov, "Dispersion properties of nonradiating configurations: finite-difference time-domain modeling," *Phys. Rev. E Stat. Nonlin. Soft Matter Phys.* **72**(3 Pt 2), 036603 (2005).
4. D. R. Smith, J. B. Pendry, and M. C. K. Wiltshire, "Metamaterials and negative refractive index," *Science* **305**(5685), 788–792 (2004).
5. B. Luk'yanchuk, N. I. Zheludev, S. A. Maier, N. J. Halas, P. Nordlander, H. Giessen, and C. T. Chong, "The Fano resonance in plasmonic nanostructures and metamaterials," *Nat. Mater.* **9**(9), 707–715 (2010).
6. W. T. Chen, P. C. Wu, C. J. Chen, H. Y. Chung, Y. F. Chau, C. H. Kuan, and D. P. Tsai, "Electromagnetic energy vortex associated with sub-wavelength plasmonic Taiji marks," *Opt. Express* **18**(19), 19665–19671 (2010).
7. S. Linden, C. Enkrich, M. Wegener, J. Zhou, T. Koschny, and C. M. Soukoulis, "Magnetic response of metamaterials at 100 terahertz," *Science* **306**(5700), 1351–1353 (2004).
8. D. Diessel, M. Decker, S. Linden, and M. Wegener, "Near-field optical experiments on low-symmetry split-ring-resonator arrays," *Opt. Lett.* **35**(21), 3661–3663 (2010).
9. W. M. Zhu, A. Q. Liu, X. M. Zhang, D. P. Tsai, T. Bourouina, J. H. Teng, X. H. Zhang, H. C. Guo, H. Tanoto, T. Mei, G. Q. Lo, and D. L. Kwong, "Switchable magnetic metamaterials using micromachining processes," *Adv. Mater. (Deerfield Beach Fla.)* **23**(15), 1792–1796 (2011).
10. W. T. Chen, C. J. Chen, P. C. Wu, S. Sun, L. Zhou, G. Y. Guo, C. T. Hsiao, K. Y. Yang, N. I. Zheludev, and D. P. Tsai, "Optical magnetic response in three-dimensional metamaterial of upright plasmonic meta-molecules," *Opt. Express* **19**(13), 12837–12842 (2011).

11. S. Zhang, Y. S. Park, J. S. Li, X. C. Lu, W. L. Zhang, and X. Zhang, "Negative refractive index in chiral metamaterials," *Phys. Rev. Lett.* **102**(2), 023901 (2009).
12. E. Plum, X. X. Liu, V. A. Fedotov, Y. Chen, D. P. Tsai, and N. I. Zheludev, "Metamaterials: optical activity without chirality," *Phys. Rev. Lett.* **102**(11), 113902 (2009).
13. C. M. Soukoulis, S. Linden, and M. Wegener, "Physics. Negative refractive index at optical wavelengths," *Science* **315**(5808), 47–49 (2007).
14. R. A. Shelby, D. R. Smith, and S. Schultz, "Experimental verification of a negative index of refraction," *Science* **292**(5514), 77–79 (2001).
15. E. Plum, V. A. Fedotov, P. Kuo, D. P. Tsai, and N. I. Zheludev, "Towards the lasing spaser: controlling metamaterial optical response with semiconductor quantum dots," *Opt. Express* **17**(10), 8548–8551 (2009).
16. V. A. Fedotov, N. Papasimakis, E. Plum, A. Bitzer, M. Walther, P. Kuo, D. P. Tsai, and N. I. Zheludev, "Spectral collapse in ensembles of metamolecules," *Phys. Rev. Lett.* **104**(22), 223901 (2010).
17. E. Plum, K. Tanaka, W. T. Chen, V. A. Fedotov, D. P. Tsai, and N. I. Zheludev, "A combinatorial approach to metamaterials discovery," *J. Opt.* **13**(5), 055102 (2011).
18. T. Li, R. X. Ye, C. Li, H. Liu, S. M. Wang, J. X. Cao, S. N. Zhu, and X. Zhang, "Structural-configured magnetic plasmon bands in connected ring chains," *Opt. Express* **17**(14), 11486–11494 (2009).
19. N. Liu, H. Liu, S. Zhu, and H. Giessen, "Stereometamaterials," *Nat. Photonics* **3**(3), 157–162 (2009).
20. K. Marinov, A. D. Boardman, V. A. Fedotov, and N. Zheludev, "Toroidal metamaterial," *New J. Phys.* **9**(9), 324 (2007).
21. N. Papasimakis, V. A. Fedotov, K. Marinov, and N. I. Zheludev, "Gyrotropy of a metamolecule: wire on a torus," *Phys. Rev. Lett.* **103**(9), 093901 (2009).
22. T. Kaelberer, V. A. Fedotov, N. Papasimakis, D. P. Tsai, and N. I. Zheludev, "Toroidal dipolar response in a metamaterial," *Science* **330**(6010), 1510–1512 (2010).
23. D. B. Burckel, J. R. Wendt, G. A. Ten Eyck, J. C. Ginn, A. R. Ellis, I. Brener, and M. B. Sinclair, "Micrometer-scale cubic unit cell 3D metamaterial layers," *Adv. Mater. (Deerfield Beach Fla.)* **22**(44), 5053–5057 (2010).
24. J. H. Cho and D. H. Gracias, "Self-assembly of lithographically patterned nanoparticles," *Nano Lett.* **9**(12), 4049–4052 (2009).

---

## 1. Introduction

Toroidal resonance is created by currents flowing on a surface of a doughnut-shaped structure along its meridians which was first reported by Zel'dovich (1957) in nuclear physics to explain the parity violation of the weak interaction force [1]. Unlike the electric dipole and magnetic dipole, the toroidal multipoles are not included in the traditional multipole expansion. Therefore, the current configuration solely generates toroidal dipole does not contribute to electric, magnetic dipole or higher multipole moments [2]. In particular, the unique property of toroidal dipole response is a non-radiating configuration which results from destructive interference between electromagnetic fields [3]. However, the toroidal dipole moment in these structures is much weaker than electric or magnetic dipole moment which is usually neglected. However, one can design an artificial sub-wavelength structure, so called metamaterials [4–6], to suppress the component of electric or magnetic dipole moment. Metamaterials are created as an array of artificial sub-wavelength structures, often exhibit unique optical properties through electric and magnetic dipole resonance which are not found in nature. Split ring resonator (SRR) is the most common structure of metamaterial, showing artificial magnetism [7–10], optical chirality [11,12], negative refraction index [13,14] and allowing for optical spectrum manipulation [15–19].

Toroidal metamaterials were first theoretically proposed by K. Marinov et al in 2007 [20] and demonstrated toroidal wire windings in a unit cell at microwave by N. Papasimakis et al. in 2009 [21]. Toroidal response results in strong dependence on the dielectric permittivity of the host medium, which can make negative index of refraction and rotate polarization state of light [20,21]. In 2010, toroidal response in microwave region was first experimentally demonstrated and separated from other multipoles by arranging four three-dimensional resonant split metallic wire loops in a unit cell of toroidal symmetry by T. Kaelberer et al. [22]. There are several possible ways to manufacture the three-dimensional SRR structures [23,24]. However, the dimension and resolution are limited in these methods. In 2011, based on our prior work, the upright U-shape SRR at nanometer scale was manufactured by using a double exposure e-beam lithographic process with high alignment technology. The

misalignment is below 10 nm [10]. It provides a promising fabrication process to investigate the toroidal response in the optical region.

In this paper, we present two types of toroidal metamaterials, functionality of which is underpinned by the resonant plasmonic responses of purposely arranged U-shaped SRRs. In the first type of metamaterial (TM1), toroidal metamolecule consists of four-up U-shaped SRRs (shown in Fig. 1(b)). In the second type of metamaterial (TM2), toroidal metamolecule consists of two-up-two-down U-shaped SRRs, as shown in Fig. 1(c). The proposed metamaterial structures that we investigate in the present work are the first example of artificial media exhibiting a clear toroidal signature in the optical part of the spectrum.

## 2. Toroidal metamolecules design and simulation results

We investigated electromagnetic response of toroidal metamaterials, infinite two-dimensional arrays of toroidal metamolecules. Figures 1(a) to 1(c) show the schematic diagrams of the unit cells of two types of toroidal metamaterials studied here together with their design parameters and the polarization state of incident light. In order to purify the resonances and eliminate the Fabry-Perot effect of the changeable thickness of MgF<sub>2</sub> in spectra, we assume that gold wires of the U-shaped SRRs are embedded in a homogeneous dielectric medium, MgF<sub>2</sub>, as simulation background.

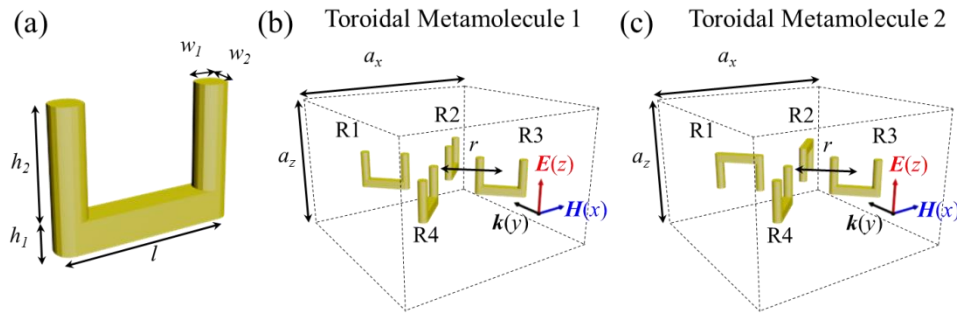


Fig. 1. Schematic diagram of the toroidal metamolecules design and the polarization configuration of incident light. (a) Feature sizes of a SRRs,  $l = 300$  nm,  $h_1 = w_1 = w_2 = 50$  nm,  $h_2 = 200$  nm. The U-shaped SRR play a role as ‘atom’ of toroidal metamolecule. (b) A unit cell of TM1 consisted by four-up U-shaped SRRs. (c) A unit cell of TM2 consisted by two-up-two-down U-shaped SRRs. In both Fig. 1(b) and 1(c), the periodicity  $a_x = 1200$  nm and,  $a_z = 800$  nm, and the distance  $r$  from the center of toroidal metamolecule to the geometric center of SRRs is 300 nm.

The metamaterials transmission spectra were obtained by solving three-dimensional Maxwell equation with the finite-element method (COMSOL Multiphysics). The refractive index of the MgF<sub>2</sub> was assumed to be 1.39 and the permittivity of gold was described by the Drude model with damping constant,  $\omega_c = 2\pi \times 6.5 \times 10^{12}$  s<sup>-1</sup> and plasma frequency,  $\omega_p = 2\pi \times 2.175 \times 10^{15}$  s<sup>-1</sup> [7].

The simulation of transmittance and reflectance spectra for TM1 and TM2 are shown in Figs. 2(a) and 2(d), in which two resonances ( $\omega_{M1}^-$ ,  $\omega_{T1}^+$  and  $\omega_{T2}^-$ ,  $\omega_{M2}^+$ ) are clearly seen. Here the resonance frequencies are  $\omega_{M1}^- = 114.7$  THz,  $\omega_{T1}^+ = 119.1$  THz,  $\omega_{T2}^- = 112.3$  THz,  $\omega_{M2}^+ = 122.1$  THz, where superscript “+” and “-” correspond to the higher and lower energy levels. The subscripts indicate character of the resonances that will be explained in the following. Comparing Fig. 2(a) with Fig. 2(d), the toroidal dipole and magnetic dipole are reversed; that is, the toroidal mode is excited at the higher frequency in the case of TM1 and at the lower frequency for TM2.

In order to study the resonances of meta-molecule quantitatively, the radiated powers of the magnitude of electric and magnetic multipoles and toroidal dipole were calculated by the induced volume current density  $\mathbf{j}$  in the metal rings of TM1 and TM2 [20–22]:

$$\text{electric dipole moment : } \quad \mathbf{P} = \frac{1}{i\omega} \int \mathbf{j} d^3r, \quad (1a)$$

$$\text{magnetic dipole moment : } \quad \mathbf{M} = \frac{1}{2c} \int (\mathbf{r} \times \mathbf{j}) d^3r, \quad (1b)$$

$$\text{toroidal dipole moment : } \quad \mathbf{T} = \frac{1}{10c} \int [(\mathbf{r} \cdot \mathbf{j}) \mathbf{r} - 2r^2 \mathbf{j}] d^3r, \quad (1c)$$

$$\text{electric quadrupole moment : } \quad Q_{\alpha\beta} = \frac{1}{i2\omega} \int \left[ r_\alpha j_\beta + r_\beta j_\alpha - \frac{2}{3} (\mathbf{r} \cdot \mathbf{j}) \delta_{\alpha\beta} \right] d^3r, \quad (1d)$$

$$\text{magnetic quadrupole moment : } \quad M_{\alpha\beta} = \frac{1}{3c} \int [(\mathbf{r} \times \mathbf{j})_\alpha r_\beta + (\mathbf{r} \times \mathbf{j})_\beta r_\alpha] d^3r, \quad (1e)$$

where  $c$  is the speed of light and  $\alpha, \beta = x, y, z$ . In Fig. 2(b) and 2(e), the radiated power of the multipole moments was calculated from the induced currents [22]:

$$I = \frac{2\omega^4}{3c^3} |\mathbf{P}|^2 + \frac{2\omega^4}{3c^3} |\mathbf{M}|^2 + \frac{4\omega^5}{3c^4} (\mathbf{P} \cdot \mathbf{T}) + \frac{2\omega^6}{3c^5} |\mathbf{T}|^2 + \frac{\omega^6}{5c^5} \sum |Q_{\alpha\beta}|^2 + \frac{\omega^6}{40c^5} \sum |M_{\alpha\beta}|^2 + O\left(\frac{1}{c^5}\right), \quad (2)$$

Using the Eq. (2), the radiated powers of TM1 and TM2 as a function of frequency are shown in Figs. 2(b) and 2(e). In Fig. 2(e), the  $x$ -component of the magnetic dipole moment  $\mathbf{M}_x$  is the strongest contribution at resonance  $\omega_{M2}^+$ , which is about 1.53 times stronger than the electric quadrupole moment. In particular, the strongest contribution to the response at resonance  $\omega_{T2}^-$  is provided by the  $z$ -component of the toroidal dipole moment  $\mathbf{T}_z$ , which radiates  $\sim 1.56$  times stronger than the  $z$ -component of the electric dipole moment  $\mathbf{P}_z$ . This result confirms that downsizing the metamolecules achieves observation of plasmonic toroidal dipole response at optical frequencies [22]. On the other hand, the radiation peak of  $\mathbf{T}_z$  and  $\mathbf{M}_x$  exchange their position as the direction of two SRRs reversed, which is presented in Fig. 2(b). In this case, the  $\mathbf{M}_x$  is still the strongest resonance at  $\omega_{M1}^-$  (more than  $\mathbf{P}_z$  by a factor of  $\sim 3.21$ ). Owing to the in-phase oscillation of induced electric quadrupole in each erected U-shaped SRR structure, the radiation power of toroidal dipole moment is smaller than that of electric quadrupole by a factor of  $\sim 5.70$  at resonance  $\omega_{T1}^+$ . However, the strength of radiated power corresponding to the  $\mathbf{T}_z$  is much stronger than that of the  $\mathbf{P}_z$  ( $\sim 2.20$  times),  $\mathbf{M}_x$  ( $\sim 7.63$  times) and magnetic quadrupole moments (more than three orders). It achieves a new plasmonic metamolecule to excite the toroidal dipole resonance at optical frequencies.

The plasmonic resonances of both metamaterial structures are excited result from the interference of several contributions. In the TM1 metamaterial the low frequency resonance is dominated by the magnetic dipole scattering, while the high frequency resonance is underpinned by resonant quadrupole and toroidal dipole responses. In contrast, in the case of TM2, toroidal scattering makes the strongest contribution to the low frequency resonance while magnetic and quadrupole responses dominate in the high frequency resonance.

Figures 2(c) and 2(f) show the hybridization model of TM1 and TM2, respectively. At first, the resonance energy of two-up U-shaped SRRs and two-down U-shaped SRRs are degenerated. Due to the coupling effect of front and back pairs of the SRRs, the energy level of degenerated resonance modes is split into toroidal and magnetic resonances. The coupling effect in the case of TM2 is stronger than that of TM1 resulted in a more distinguished energy splitting.

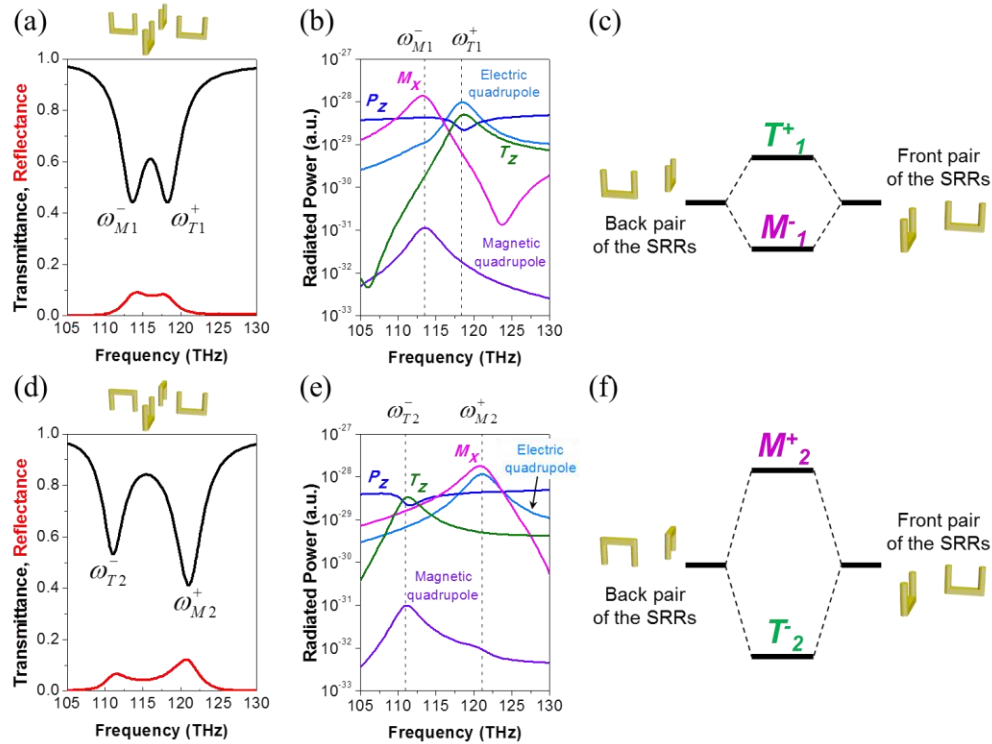


Fig. 2. Simulated transmittance and reflectance spectra of TM1 (a) and TM2 (d). The superscript “+” and “-” correspond to the higher and lower energy levels of each TM. The subscript “M” and “T” corresponding to magnetic resonance and toroidal resonance, respectively. Dispersion of radiated powers of various multipole moments for TM1 (b) and TM2 (e). Hybridization model of metamolecules for TM1 (c) and TM2 (f). The resonance energy of two-up U-shaped SRRs and two-down U-shaped SRRs are degenerated. Due to the coupling effect of SRRs, the energy level of degenerated resonance mode are split into toroidal and magnetic resonance. It’s notably that the splitting of energy level in the case of TM1 is larger than that of TM2, and the toroidal resonance of TM1 is excited at higher frequency than that of TM2.

In order to explore the character of each resonance, numerical simulations of fields and phenomena of dipoles interaction of the resonances are carried out as below. Magnetic energy and field distributions at the relevant resonance modes of TM1 and TM2 are shown in Fig. 3. The first row of Fig. 3 shows the magnetic field distribution (shown in black line) and the logarithm of magnetic energy (shown in color map). Due to the excitation of the plasmonic resonances, the magnetic energy is enhanced in the gap of the resonance rings for both toroidal and magnetic resonances. The magnetic field distribution shows ring-like and dipole-like profile corresponding to toroidal and magnetic resonance, respectively. The magnetic energy and field distribution of resonance mode  $\omega_{T1}^+$  is similar to that of  $\omega_{T2}^+$ , as well as the relation between  $\omega_{M1}^-$  and  $\omega_{M2}^-$ . The second row shows the  $z$ -component current density (shown in color scale). According to the current density distribution, the schematic diagram of the induced dipoles was shown in the third row. The incident light induces magnetic dipole ( $\mathbf{m}$ ) in each of SRRs, which makes current density ( $\mathbf{j}$ ) flow on the surface of each SRRs, and makes the  $z$ -component current density on the boundary of arms with different direction. There is a phase delay when the external wave passing through the front and back pairs of ring resonators. Thus, the induced magnetic dipoles of each resonator pair can be composed into anti-phase oscillating results in the ring-like profile of magnetic dipoles which create toroidal

resonance ( $T$ ). In contrast, the induced magnetic dipoles of each resonator pair with in-phase oscillation produced magnetic resonance ( $M$ ) [22].

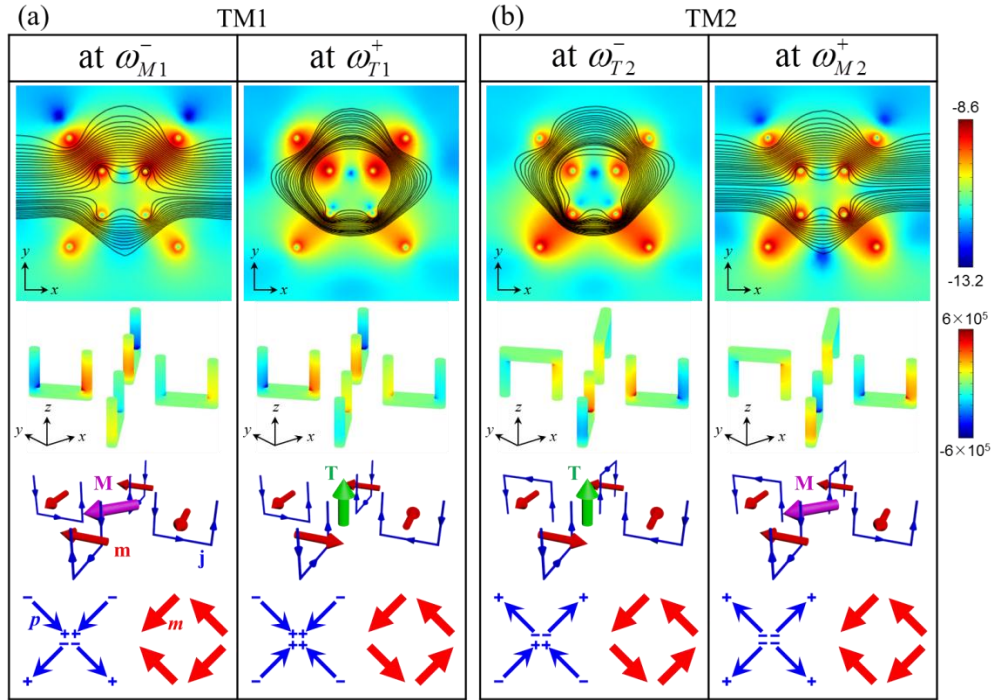


Fig. 3. Magnetic energy (color map, in logarithm scale), streamline of magnetic field (black line) and current density of z-component distributions (shown in color in second row) at respective resonances for the TM1 (a) and TM2 (b). The third row: schematic diagram of generated magnetic resonance ( $M$ ) and toroidal resonance ( $T$ ) in the case of TM1 and TM2. The magnetic dipole and surface current of a SRR are shown in red and blue arrow, respectively. The lowest row: schematic diagram of the electric (in blue arrow) and magnetic (in red arrow) dipoles interactions, which can explain the resonant modes in higher or lower energy.

The last row of Fig. 3 shows the separation of positive (+) and negative (-) charges from current density and their corresponding electric and magnetic dipoles ( $p$  and  $m$ ). Because of the electric and magnetic dipoles coupling, the magnetic dipole resonance of a single SRR is split into magnetic and toroidal resonances by integrating four SRRs together. Subsequently, according to the calculation of energy of the electric and magnetic dipoles interaction in Ref [18], the longitudinal electric dipoles show anti-phase (in-phase) at higher (lower) energy. The transverse magnetic dipoles align in-phase (anti-phase) at higher (lower) energy. In the case of TM1, the toroidal resonance is excited at the higher frequency than the magnetic resonance because the longitudinal electric dipole pairs (front and back pairs of the SRRs) show anti-phase and in-phase configuration, respectively. As a consequence, the electric dipoles interaction plays a dominated role on determining the energy level of resonant modes.

The energy splitting in the case of TM2 is stronger than that of TM1 because the arrangement of magnetic and electric dipoles interaction corresponding to the different interaction energy. For example, in the case of TM2, the toroidal resonance corresponds to in-phase longitudinal electric and anti-phase transverse magnetic dipoles interaction (see the last row of Fig. 3(b)), which are both in stable and lower energy components. As a result, the interactions in each of electric and magnetic dipoles contribute positively in the TM2. In contrast, the toroidal resonance in the case of TM1 corresponds to the higher energy of longitudinal electric dipoles interaction (anti-phase) but lower energy of transverse magnetic

dipoles interaction (anti-phase). The electric and magnetic interactions work against one another in TM1, which leads to smaller spectral splitting.

### 3. Analysis of the coupling mechanics

To further quantitatively clarify the dipole coupling and energy splitting, a theoretical analysis based on four coupled LC circuits is used to analyze the phenomenon of reversed resonance mode. The resonance frequency of single ring is  $\omega_0 = (LC)^{-1/2} = 116.7$  THz and the Lagrangian [18,19] of the coupled system is written as

$$\begin{aligned} \Gamma = & \frac{L}{2}(\dot{Q}_1^2 + \dot{Q}_2^2 + \dot{Q}_3^2 + \dot{Q}_4^2) - \frac{L}{2}\omega_0^2(Q_1^2 + Q_2^2 + Q_3^2 + Q_4^2) \\ & + \frac{L'}{2}(\dot{Q}_1 + \dot{Q}_2 - \dot{Q}_3 - \dot{Q}_4)^2 \\ & - M_H\dot{Q}_1\dot{Q}_3 - M_H\dot{Q}_2\dot{Q}_4 - M_E\omega_0^2Q_1Q_3 - M_E\omega_0^2Q_2Q_4, \end{aligned} \quad (3)$$

where  $Q_i$  ( $i = 1,2,3,4$ ) are oscillating charges in the respective SRRs R1 to R4; the first two terms result from the inductances and the capacitors;  $L'$  is the community inductance from the inner four arms of molecules;  $M_E$  and  $M_H$  are the coupling coefficients of the electric and magnetic dipoles interactions. For  $Q_1 = Q_3 = Q_a$ ,  $Q_2 = Q_4 = Q_b$ ,

$$\begin{aligned} \Gamma = & L(\dot{Q}_a^2 + \dot{Q}_b^2) - L\omega_0^2(Q_a^2 + Q_b^2) + 2L'(\dot{Q}_a - \dot{Q}_b)^2 \\ & - 2M_H\dot{Q}_a\dot{Q}_b - 2M_E\omega_0^2Q_aQ_b. \end{aligned} \quad (4)$$

Subsequently, adopting the root form of  $Q_i = A_i \exp(i\omega t)$  and by solving the Euler-Lagrange equations  $\frac{d}{dt} \frac{\partial \Gamma}{\partial \dot{Q}_i} - \frac{\partial \Gamma}{\partial Q_i} = 0, (i = a, b)$ , the eigen-frequencies of these toroidal metamolecules can be obtained as

$$\begin{cases} \omega_M = \omega_0 \sqrt{\frac{1 + \kappa_E}{1 - \kappa_H}}, & \text{with } Q_a = Q_b \\ \omega_T = \omega_0 \sqrt{\frac{1 - \kappa_E}{1 + 4\eta + \kappa_H}}, & \text{with } Q_a = -Q_b, \end{cases} \quad (5)$$

where  $\eta = L'/L$ ,  $\kappa_E = M_E/L$  and  $\kappa_H = M_H/L$  are the normalized coupling coefficients of the overall interactions, respectively. We suppose that the electric coupling coefficient changes to  $\kappa_{E1}$  and  $\kappa_{E2}$  in the different connection cases of TM1 and TM2, while  $\eta$  and  $\kappa_H$  are the same. That is to say,

$$\begin{cases} \omega_{M1}^- = \omega_0 \sqrt{\frac{1 + \kappa_{E1}}{1 - \kappa_H}}, \quad \omega_{T1}^+ = \omega_0 \sqrt{\frac{1 - \kappa_{E1}}{1 + 4\eta + \kappa_H}}, & \text{for TM1} \\ \omega_{M2}^+ = \omega_0 \sqrt{\frac{1 + \kappa_{E2}}{1 - \kappa_H}}, \quad \omega_{T2}^- = \omega_0 \sqrt{\frac{1 - \kappa_{E2}}{1 + 4\eta + \kappa_H}}, & \text{for TM2.} \end{cases} \quad (6)$$

Since the four resonance frequencies of TM1 and TM2 are obtained from simulated transmittance of Fig. 2, the normalized coupling coefficients can be calculated with those given resonance frequencies as  $\eta = -0.0029$ ,  $\kappa_{E1} = -0.0912$ ,  $\kappa_{E2} = 0.0298$  and  $\kappa_H = 0.0592$ . The coefficients of magnetic coupling term  $\kappa_H$  for these two cases are both positive, while

that of electric coupling term  $\kappa_E$  is negative for four-up SRRs (TM1) and positive for two-up-two-down SRRs (TM2). The absolute value of  $\kappa_{E1}$  is larger than  $\kappa_{E2}$ , which is similar with [18]. The electric coupling is stronger than magnetic coupling in the case of TM1, which provides evidence that electric dipoles interaction plays the dominated role of resonant frequencies. In the case of TM2, the magnetic coupling is stronger than electric coupling. In both of these two cases, the community inductance from the inner four arms of molecules is many smaller than the coupling coefficients of the dipoles interactions.

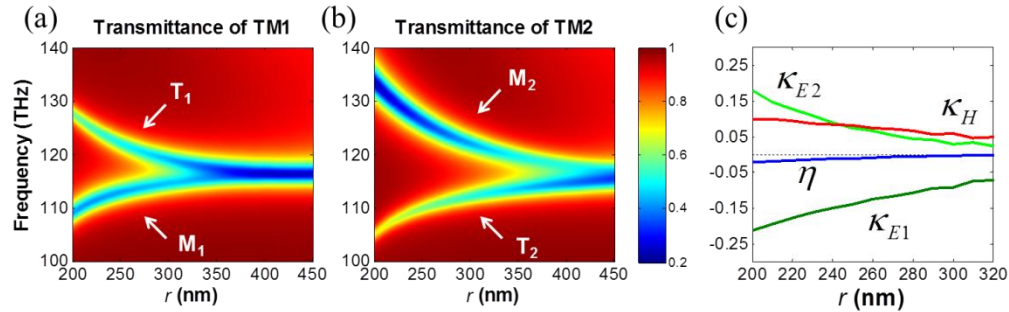


Fig. 4. Simulated transmission spectra as a function of radius  $r$  of TM1 (a) and TM2 (b). (c) The normalized coupling coefficients as a function of radius  $r$  obtained from the resonance frequencies in (a) and (b).

Furthermore, we study the energy splitting of magnetic and toroidal resonances by decreasing the distance  $r$  of four SRRs from 450 nm to 200 nm, which means increasing the couple strength of four SRRs in the TM1 and TM2. The transmittance spectra as a function of  $r$  are shown in Fig. 4(a) and 4(b), respectively. In the case of  $r = 450$  nm, due to weak coupling of four SRRs, the energy splitting is hardly observed. When  $r$  is decreased, the coupling becomes stronger, the phenomenon of energy splitting is more distinct, resulting in the toroidal resonance (the higher frequency branch of TM1 and lower frequency branch of TM2 in Fig. 4(a) and 4(b)). However, the toroidal resonances become weaker as  $r$  is continuously decreased. For example, in the case of  $r = 200$  nm, the toroidal mode is too weak to be observed. As a result, the toroidal mode is created by increasing the coupling effect of each ring resonators, but the intensity of toroidal resonance is decreased while the coupling effect of each SRRs become too stronger. Figure 4(c) shows the numerical calculation results of normalized coupling coefficients ( $\kappa_{E1}$ ,  $\kappa_{E2}$ ,  $\kappa_H$  and  $\eta$ ) as a function of distance  $r$  obtained by solving the Eq. (6) with the resonance frequency of TM1 and TM2 in Figs. 4(a) and 4(b). The absolute value for the parameters  $\kappa_{E1}$ ,  $\kappa_{E2}$ ,  $\kappa_H$  and  $\eta$  increase as the radius  $r$  decreased. These parameters provide a quantitative value on the magnitude of the electric/magnetic dipole coupling.

#### 4. Summary

In summary, we have presented two new related classes of plasmonic metamaterial that show profound resonant toroidal responses at optical frequencies. Computer simulations and analytical modeling revealed the toroidal responses in the plasmonic metamaterial composed of arrangements of U-shaped resonators can be fine controlled by changing the related position between resonators. Our results clearly indicate that achieving toroidal response at optical frequencies shall be possible with metamaterial arrays that can be manufactured by existing nanofabrication technologies. The manufacture of plasmonic toroidal mode in TM1 will be more easily to achieve since the easier fabrication of upright U-shape SRR than the inverted one. This work providing a way toward promising applications based on toroidal resonance at optical frequencies.

## **Acknowledgments**

The authors are grateful to Nikitas Papasimakis for fruitful discussions. The authors thank financial aids from National Taiwan University, National Science Council, Taiwan under grant numbers 99-2911-I-002-127, 99-2120-M-002-012, 100-2923-M-002-007-MY3 and 100-2120-M-002-008. Authors are grateful to EPSRC, UK and the Royal Society, London, the National Center for Theoretical Sciences, Taipei Office, Molecular Imaging Center of National Taiwan University and National Center for High-Performance Computing, Taiwan for their support.